Rare Metal Materials and Engineering
Volume 50, Issue 10, October 2021
Available online at www.rmme.ac.cn

Science Press

Cite this article as: Song Xiaoxiao, Zhou Lv, Li Ke, et al. Influence of Hot Corrosion on Precipitation of δ Phase and Tensile Properties of GH4169 Superalloy[J]. Rare Metal Materials and Engineering, 2021, 50(10): 3427-3436.

ARTICLE

Influence of Hot Corrosion on Precipitation of δ Phase and Tensile Properties of GH4169 Superalloy

Song Xiaoxiao[1], Zhou Lv[1], Li Ke[1], Ren Kaixu[2], Wang Jiayu[2], Wang Xin[2]

[1] Sino-European Institute of Aviation Engineering, Civil Aviation University of China, Tianjin 300300, China; [2] China Automotive Technology and Research Center Co., Ltd, Tianjin 300300, China

Abstract: The hot corrosion behavior of the superalloy GH4169 were analyzed in the salt mixture of 75Na_2SO_4+ 25NaCl (wt%) at 650, 750 and 850 °C for 50, 75 and 100 h. Then the precipitation of δ phase and tensile properties of the superalloy at ambient temperature were investigated. Results show that with increasing the heat treatment temperature, the ultimate tensile strength (UTS) and yield strength (YS) of the alloy exhibit a drastic degradation while elongation improves significantly. The needle-shaped δ phase precipitated at the grain boundaries can enhance the strength of the superalloy, and cause intergranular brittle fracture. As a result, the ductility of the superalloy is reduced after exposure at 750 °C. The corrosion mechanism of the alloy conforms to type-II hot corrosion at 650 and 750 °C while to type-I hot corrosion at 850 °C. Both kinds of corrosion can form a corrosion layer and promote the δ phase precipitation.

Key words: hot corrosion; GH4169 superalloy; δ phase; tensile property

GH4169 superalloy is extensively employed as the vital components of high-temperature load-bearing parts (e. g., blades, aerospace engines and gas turbines) for its prominent mechanical characteristics and high corrosive resistance at high temperature[1-5]. The strength of GH4169 alloy primarily originates from coherent body-centered tetragonal γ″ (Ni_3Nb) precipitates and is slightly brought by some face-centered cubic structured coherent γ′ [Ni_3(Al, Ti)] precipitates[6-11]. The equilibrium phase corresponding to the metastable γ″ precipitates is the orthorhombic incoherent δ phase, capable of transforming from γ″ phase under the exposure over 650 °C[12-14]. Moreover, because of the same composition of γ" and δ, the growth of the δ phase causes the γ″ phase to reduce, thereby visibly degrading the mechanics-related characteristics of the superalloy[15].

Owing to the broad application of GH4169 superalloy, it is expected to withstand aggressive service conditions (e. g., complex hot corrosion environment and high temperature). For instance, GH4169 alloy is commonly exposed to molten salt, like NaCl and Na_2SO_4 during service, causing severe hot corrosion due to salt deposition on the surface[16,17]. According to the temperature of the service, hot corrosion is generally classified as high-temperature hot corrosion (800~950 ° C, type-I) and low-temperature hot corrosion (600~750 °C, type-II) [18,19]. Type-I hot corrosion originates from basic fluxing, alloy induced acidic fluxing or sulphidation, but type-II hot corrosion results from gas induced acid fluxing or sulphidation[20]. In type-I hot corrosion, Na_2SO_4 is in a molten state, while it forms eutectic of Na_2SO_4-MSO_4 (*M*=Ni, Co, Fe) in the type-II corrosion. The NaCl in the marine environment reacts with the sulfur in the fuel in the combustion chamber of the turbine and induces corrosion of the turbine parts[21].

Recent studies have explored the hot corrosion behavior and mechanical properties of GH4169 alloy. Anderson et al[15] analyzed the relationships between δ phase precipitation and mechanical properties in IN718 superalloy. According to the study of Mahobia et al[22], with increasing the thickness of slat coating in different molten salt mixtures at 550 and 650 °C, the hot corrosion rate of IN718 superalloy increases. Zhang et al[23] suggested that with increasing the content of δ phase, the plasticity of the specimen at elevated temperatures decreases. Lin et al[24] demonstrated that by facilitating the dynamic

Received date: October 04, 2020
Foundation item: Fundamental Research Funds for the Central Universities of Civil Aviation Universities of China (3122019177)
Corresponding author: Song Xiaoxiao, Master, Sino-European Institute of Aviation Engineering, Civil Aviation University of China, Tianjin 300300, P. R. China, Tel: 0086-22-24092872, E-mail: xxsong@cauc.edu.cn

recrystallization with subsequent straining process, δ phase can expedite the flow softening. In addition, according to Ye et al[25], the excessive needle or short rod shaped δ phase accounts for the reduction of elongation. Thus, the mechanical properties[11,26,27], corrosion mechanisms[28,29], and microstructural evolution[30-32] of typical nickel-based superalloys have been reported by uniaxial tension/fatigue/creep experiments in sundry molten salt mixtures at different temperatures. Furthermore, the emphasis of several researchers was the influences of hot deformation on precipitation of δ phase[33,34]. As evidently suggested from the mentioned studies, the internal relationships between hot corrosion, precipitation of δ phase and reduction of tensile properties of GH4169 have aroused rare interest. Thus, the effect of hot corrosion on the tensile behavior, precipitated phases and hot corrosion mechanism of GH4169 requires in-depth analysis.

In this study, the effect of hot corrosion on precipitation of δ phase and tensile properties of GH4169 was investigated to enhance the tensile properties and hot corrosion resistance, as well as to predict the service life of GH4169 alloy. The salt mixture of 75Na_2SO_4+25NaCl (wt%) was adopted to simulate the atmosphere of combustion chamber of a gas turbine engine, in order to corrode GH4169. The microstructure and tensile properties of uncorroded specimens under the identical treatment conditions of aging time and temperatures were compared. Moreover, the intrinsic relationships between the hot corrosion, tensile properties and precipitated phases were elucidated.

1 Experiment

1.1 Materials

Beijing Institute of Aerial Materials provided the GH4169 rods with 20 mm in diameter, which were chemically composed (wt%) of Ni52.46, Cr18.54, Nb5.45, Mo3.05, Ti0.87, Al-0.53 and Fe balance (wt%). Based on HB5143-96, they were divided to produce small rod-like tensile specimens. Moreover, part of the GH4169 superalloy was processed into a quarter cylinder with a radius of 10 mm and a thickness of 5 mm, which acts as the metallographic specimens. Fig. 1 illustrates the specific dimensions of the tensile specimen.

1.2 Hot corrosion treatment

In the present study, the cylindrical tensile specimens were subjected to corrosion heat treatment by a salt mixture consisting of 200 g 75Na_2SO_4+25NaCl (wt%) with the crucible method. Thermal exposure was performed at 650, 750 and 850 ℃ for 50, 75 and 100 h. The hot corrosion was performed in an air furnace, and the heat treatment was started as soon as the tensile specimens were placed into the furnace. To keep the metallographic phase of the tensile specimen unchanged after the heat treatment, the tensile specimens after the heating were water quenched. To determine the hot corrosion effect, the reference group without corrosion heat treatment was established.

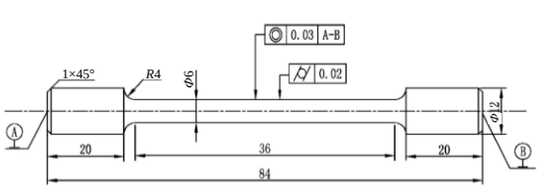

Fig.1 Rod-like tensile specimen

1.3 Tensile test and preparation of metallographic specimens

Uniaxial tensile tests were performed on Instron 5982 electronic universal material testing machine at the ambient temperature with a mechanical extensometer, which has a maximum displacement of 2.5 mm. Since the range of the extensometer was limited, the strain rate was assessed until the extensometer was removed after 1%. Former tensile tests proved that the interruption does not affect the accuracy. For each heat treatment condition, tensile were repeated two times. The average values were obtained for analysis. To delve the impact of hot corrosion on tensile behavior, the microstructures and fracture surfaces were analyzed by the scanning electron microscope (SEM) and the energy-dispersive spectrometer (EDS). The metallographic specimens were prepared by standard grinding and mechanically polishing procedures. Subsequently, they were etched for 7 min in a corrosive liquid composed of 1.5 g $CuSO_4 \cdot 5H_2O$+20 mL C_2H_5OH+20 mL HCl.

2 Results and Discussion

2.1 Tensile behavior

The tensile properties of the studied superalloy GH4169 after all the heat treatment are illustrated in Fig. 2. It shows that the mechanical properties exhibit a sensitivity to hot corrosion and temperature. With the rise of the heating temperature, both the yield strength (YS) and the ultimate tensile strength (UTS) monotonically decrease sharply. Furthermore, with the prolonged heat treatment time, YS and UTS show a slight decrease. Additionally, under the temperature of 650 and 850 ℃, YS and UTS of uncorroded specimens generally exceed those of the corroded specimens. An opposite behavior can be observed at 750 ℃, namely, the YS and UTS of corrosive specimens are almost higher than those of noncorrosive specimens.

The tendency of the elongation to failure of the uncorroded specimens is consistent with that of corroded specimens, as presented in Fig. 3. However, the elongation of noncorrosive specimens is nearly greater compared with that of corrosive specimens. Basically, with increasing the heating treatment temperature, the elongation of the specimens increases continuously. The variation of elongation to fracture is not obvious when the thermal exposure time increases at the temperature of 650 and 850 °C, except corrosive specimens at 850 °C, which displays an obvious downward trend. In contrast, the 750 °C heat treatment displays a significant trend of increasing with the rise of the heat treatment duration. It is noteworthy that the elongation of the specimens at 750 °C for

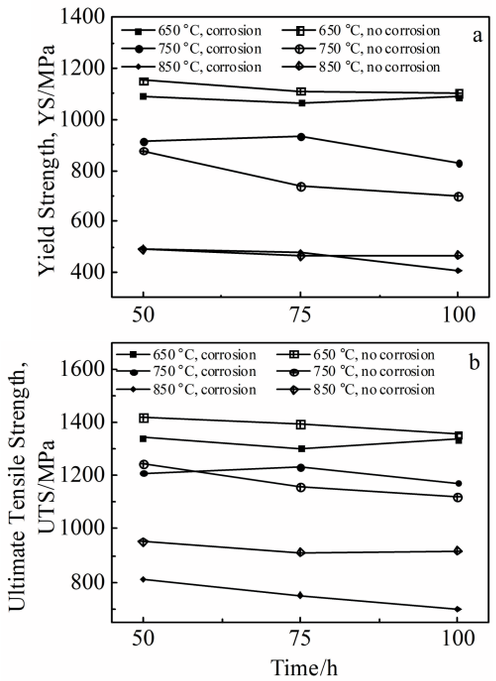

Fig.2 YS (a) and UTS (b) variation curves of GH4169 superalloy under different heat treatments

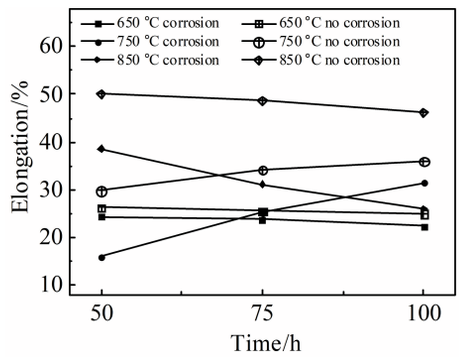

Fig.3 Elongation variation curve of GH4169 superalloy under different heat treatments

50 h is close to or smaller than that of the specimens at 650 °C for 50 h.

2.2 Tensile fracture morphology

To identify the fracture characteristics, the fracture morphology of the fiber region of the uncorroded specimens were observed. Overall, from Fig. 4a and Fig. 4b, it can be indicated that the fracture surfaces exhibit typical equiaxed dimples at the temperature of 650 and 750 ℃, which form since the plane is perpendicular to the force loading direction. For the material aged at 850 ℃, some noticeable elongated dimples are distributed on the fracture surface (Fig.4c), which are caused by considerable δ phase at 850 °C, and the fracture direction is along the δ precipitation direction, thereby elongating the dimples.

The microstructures of the tensile fracture fiber zone of the corrosion heat treated specimens are illustrated in Fig. 5. The morphology is different from that of the uncorroded specimens. At 650 ℃, compared with uncorroded heat treated specimens, the number and size of tiny voids in the fiber region remarkably increase. Different from other conditions, grains can be easily observed on the fracture surface, almost without dimples (Fig. 5b). As indicated from the mentioned typical fracture features, failure takes place by mixture of ductile fracture and intergranular fracture (primarily intergranular fracture) at 750 ℃. The fracture morphology at 850 ℃ is similar to that of uncorroded specimens at 850 ℃; however, compared with the uncorroded specimens, its dimples and tiny voids are larger, denser and more abundant in the whole.

2.3 Metallographic morphology

Fig. 6 illustrates the general sequence of precipitation after the non-corrosion isothermal treatment. It can be observed that with increasing the heat treatment temperature and time under noncorrosive conditions, the distribution and morphology of δ precipitates vary considerably. The characteristics of δ phase are almost similar according to Fig. 6a~6c. The notable phenomenon is significantly few granular and short rod-shaped δ particles in grain boundaries regardless of the duration time. As shown in Fig. 6d, a very small amount of intergranular δ phases are reported at certain grain boundaries usually in the form of globular particles. Moreover, most of grain boundaries remain free of δ precipitates. With the extension of treatment time, a relatively

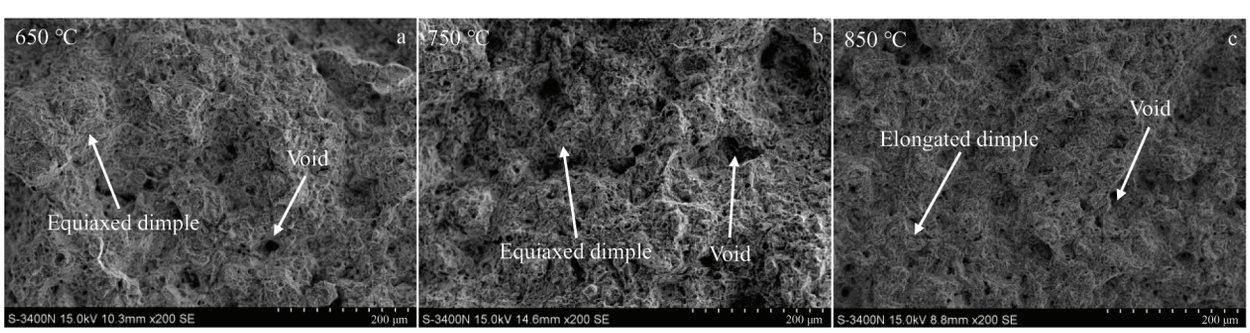

Fig.4 Morphologies of fiber areas in tensile fractures after non-corrosion heat treatment at different temperatures: (a) 650 ℃, (b) 750 ℃, and (c) 850 ℃

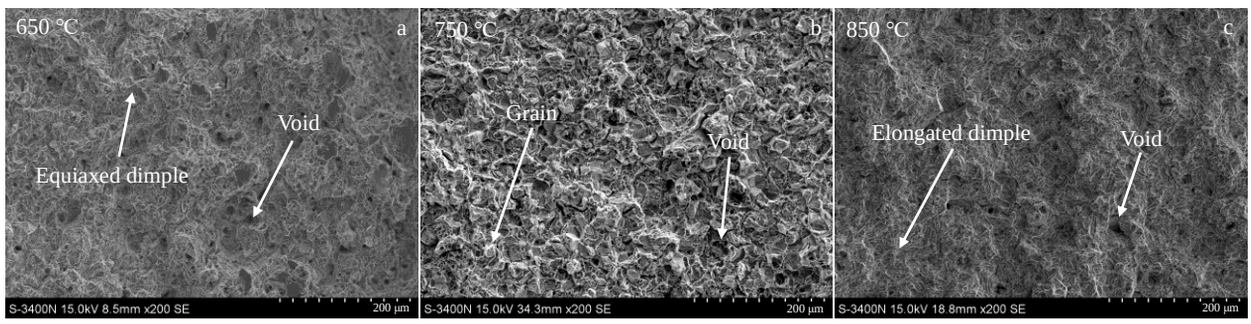

Fig.5 Morphologies of fiber areas in tensile fractures after corrosion heat treatment at different temperatures: (a) 650 ℃, (b) 750 ℃, and (c) 850 ℃

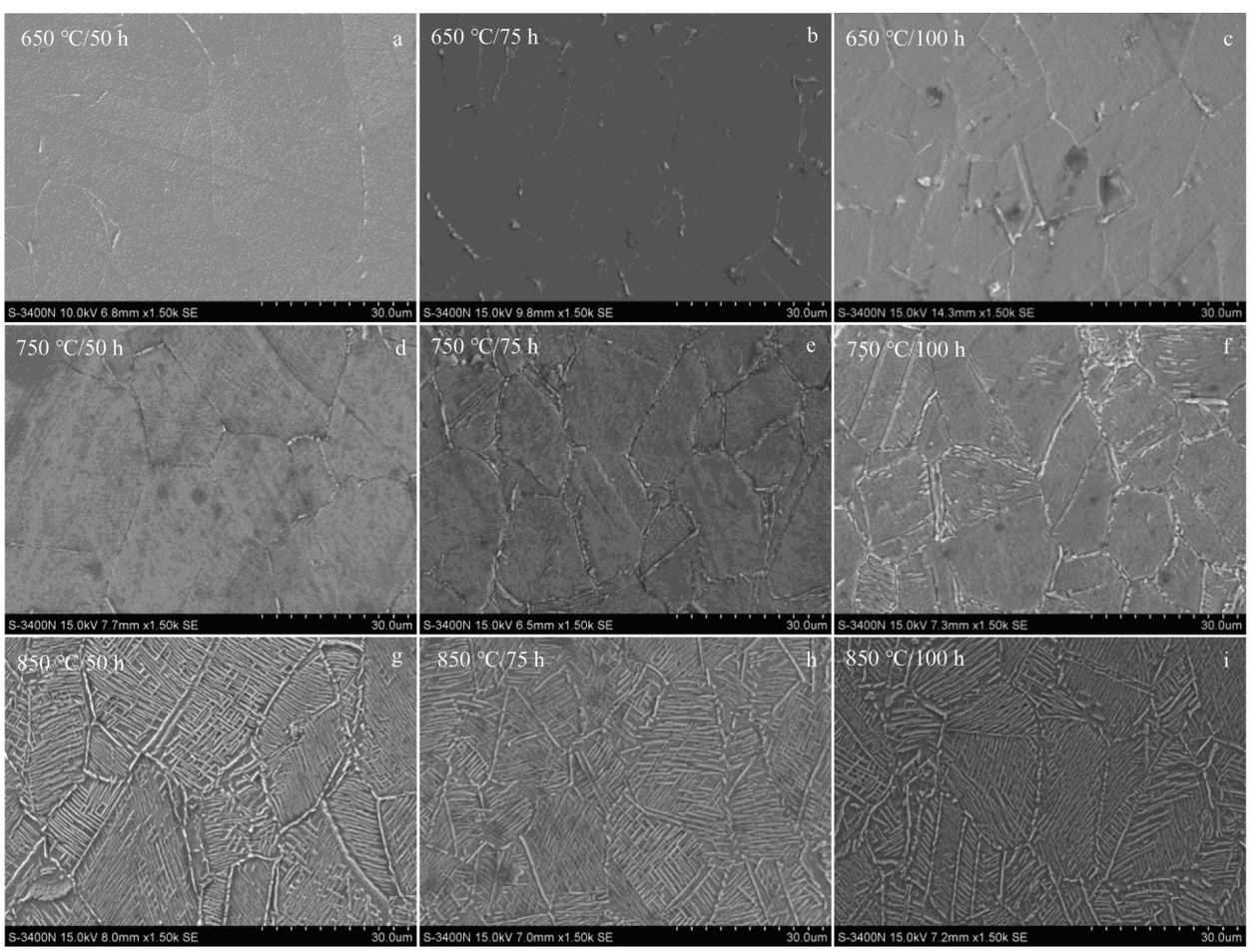

Fig.6 Microstructures of GH4169 superalloy after non-corrosion heat treatment under different conditions: (a) 650 ℃, 50 h; (b) 650 ℃, 75 h; (c) 650 ℃, 100 h; (d) 750 ℃, 50 h; (e) 750 ℃, 75 h; (f) 750 ℃,100 h; (g) 850 ℃, 50 h; (h) 850 ℃, 75 h; (i) 850 ℃, 100 h

considerable δ phases present in grain boundaries, as shown in Fig. 6e, which are evolved into the continuous needle-like δ phase beyond the precipitation of particles in a given grain. When the treatment duration reaches up to 100 h, particle-like and short plate-like δ phase already precipitate in grains, indicating an obvious coarsening of the preexisting δ precipitates. At the thermal exposure temperature of 850 ℃, in spite of the duration time, there are two distinguished types of precipitates, i.e., granular- and needle-shaped along the grain boundaries, and lamellar and clusters of parallel plates throughout the grains. Under the mentioned condition, the quantity of intragranular precipitates is more pronounced compared with that of the intergranular ones.

The typical microstructures of the GH4169 specimens after different corrosion heat treatments are presented in Fig. 7. Under the same heat treatment conditions, the δ phase number

of corroded specimens is greater compared with that of uncorroded specimens. In Fig. 7a~7c, considerable δ phases exist at the grain boundaries, and most of them are circular or short rod-shaped while only few particles have no clean grain boundaries. At 750 ℃, δ phases turn out to be obviously coarsened, and some δ phases are elongated and needle-shaped cross over the whole grains. The distribution of δ phase at 850 ℃ is similar to that under 850 ℃ non-corrosion heat treatment; its precipitation, however, is found to be larger, denser and more abundant than that of the uncorroded specimen. The δ phases running through the entire grain parallel with the grain are interlaced, and the amount of intragranular precipitates is proved to be preponderant over those intergranular.

2.4 Corrosion oxide layer morphology

The morphologies of the oxide layer of the uncorroded metallographic specimens are illustrated in Fig.8. With the rise of the treatment temperature, the thickness of the oxide layer shows a slight variation, demonstrating that GH4169 displays outstanding oxidation resistance without corrosion.

The outermost oxide layer and the inner corrosion layer are separated by a dividing line in Fig. 9, while the delamination exists. With increasing the heat treatment time, the thickness of the corrosion layer shows a remarkable elevation. The oxide layer has a tendency to peel off and then a gap between the oxide layer and the corrosion layer is formed. Fig. 9 illustrates the line scan results, demonstrating that the oxide layer is primarily composed of Cr, Fe elements and their oxides. With the variation of time, the S element is primarily identified in the corrosion layer at first (line 1); next, the content is peaked at outmost layer (line 2); lastly, and it becomes the original state but violently fluctuates at the corrosion layer (line 3). However, only a small amount of Cl element is relatively evenly distributed on both layers, besides the peak which is formed at the outmost oxide layer, as depicted in line 3.

The oxide layers of the specimens in Fig. 10 peel off completely, and only the exposed corrosion layer can be identified, as compared with Fig. 9. With extending the heat treatment time, the corrosion layer becomes gradually loose and porous. Moreover, corrosion products emerge between the corrosion layer and the matrix, which are most noticeable in line 6 and increase the thickness of corrosion layer. According to the line scan results in Fig. 10, the S element is primarily

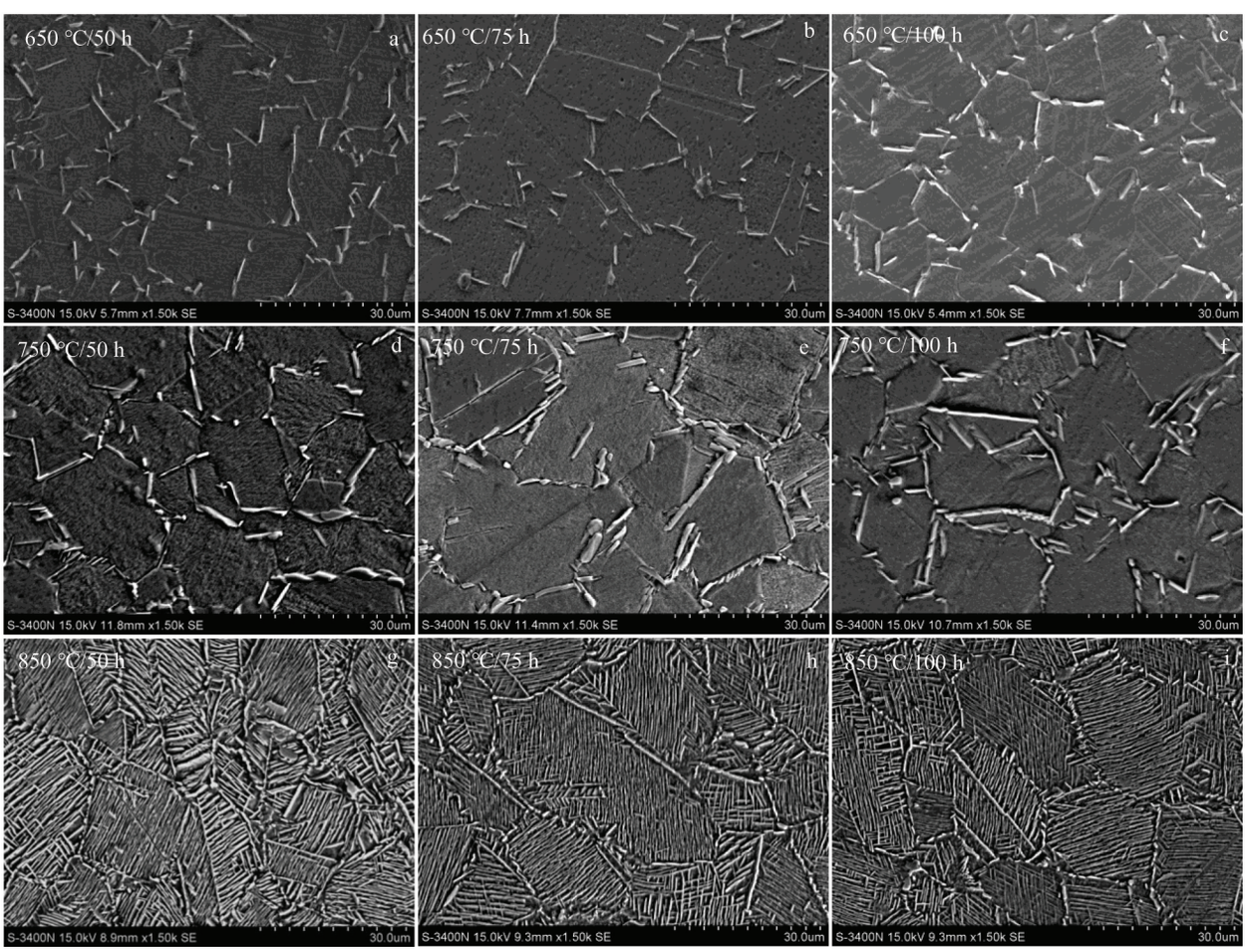

Fig.7 Microstructures of GH4169 superalloy after corrosion heat treatment: (a) 650 ℃, 50 h; (b) 650 ℃, 75 h; (c) 650 ℃, 100 h; (d) 750 ℃, 50 h; (e) 750 ℃, 75 h; (f) 750 ℃,100 h; (g) 850 ℃, 50 h; (h) 850 ℃, 75 h; (i) 850 ℃, 100 h

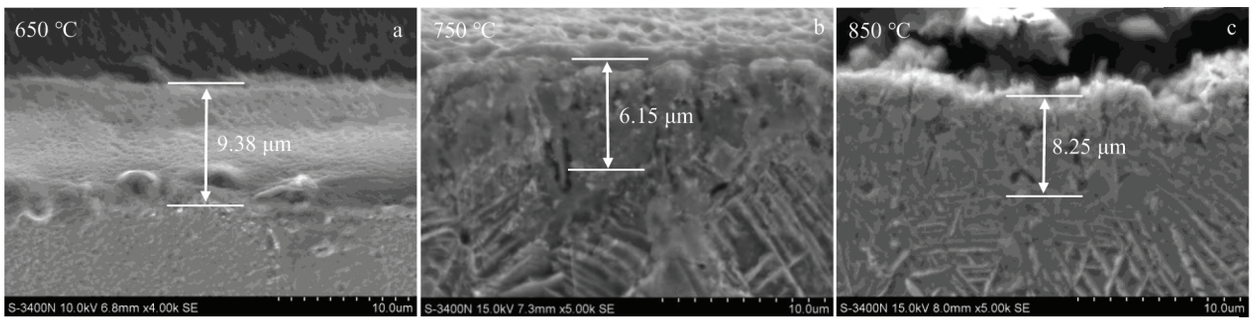

Fig.8 Morphologies and thickness of oxide layer of non-corrosion heat treatment specimens at different temperatures: (a) 650 °C, (b) 750 °C, and (c) 850 °C

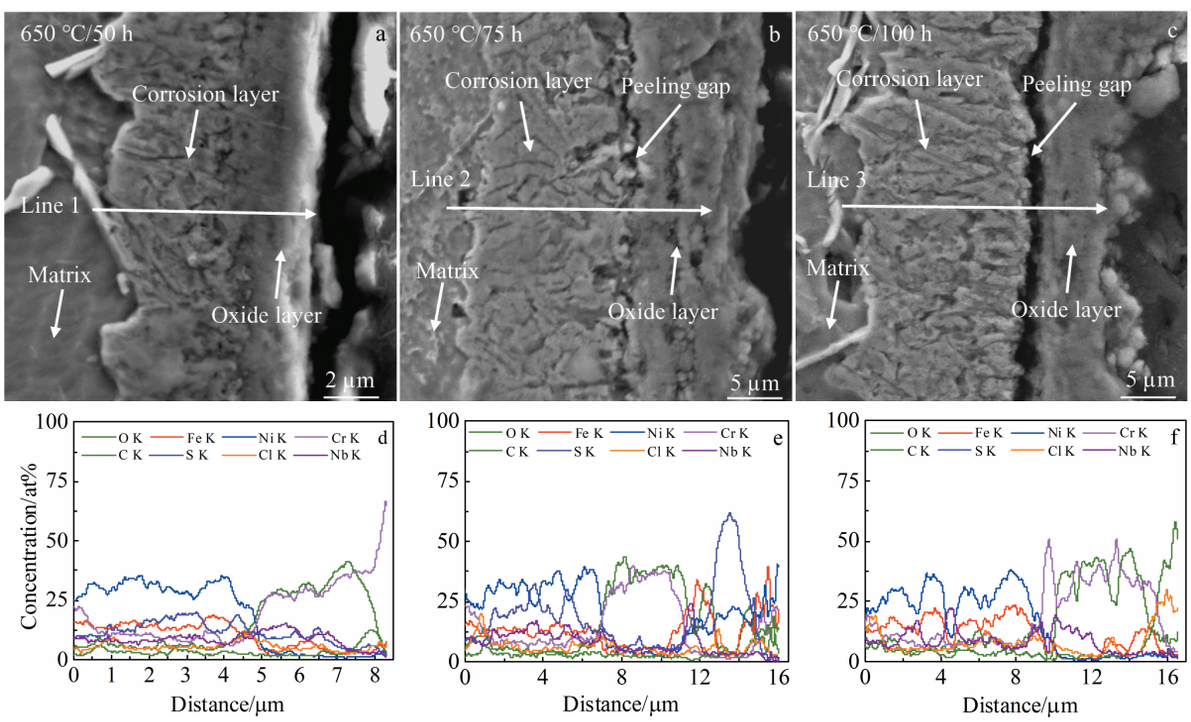

Fig.9 Corrosion oxidation layer morphologies (a~c) and line scan results along line 1 (d), line 2 (e) and line 3 (f) of hot corrosion-treated specimens at 650 °C for different time

distributed in the corrosion layer near the matrix and Cl element is detected in corrosion layer at first (line 4). With the continuous corrosion, the outer side of the corrosion layer shows a gradually loose change, and the contents of Cl and S elements increase (line 5). Lastly, the novel corrosion layer is formed; meantime, considerable S elements are detected in this layer; on the original corrosion layer, the content of O element, however, is noticeably high (line 6). It is demonstrated that the corrosion products formed by sulfidation are finally oxidized and make the corrosion layer porous.

Similar to Fig. 10, only the exposed and thicker corrosion layer can be observed in Fig. 11. At 850 °C, the corrosion mechanism follows type-I rather than type-II; the corrosion process is faster and the layer is thicker. The results of the line scan are also illustrated in Fig. 11. Such as line 6, considerable O can be detected in the incompletely peeled corrosion layer, but the content is small in the unpeeled corrosion layer (line 7). As the corrosion process continues, the S element is extensively distributed in the corrosion layer and the content peaks appear in some places, but the Cl element is primarily distributed near the matrix (line 8). This distribution is maintained (line 9), which illustrates that the corrosion process is a cycle of a series of processes and will eventually gradually stabilize.

2.5 Discussion

2.5.1 Influence of hot corrosion on tensile properties and precipitation of δ phase

Fig.2a shows that in a given heat treatment duration, the YS

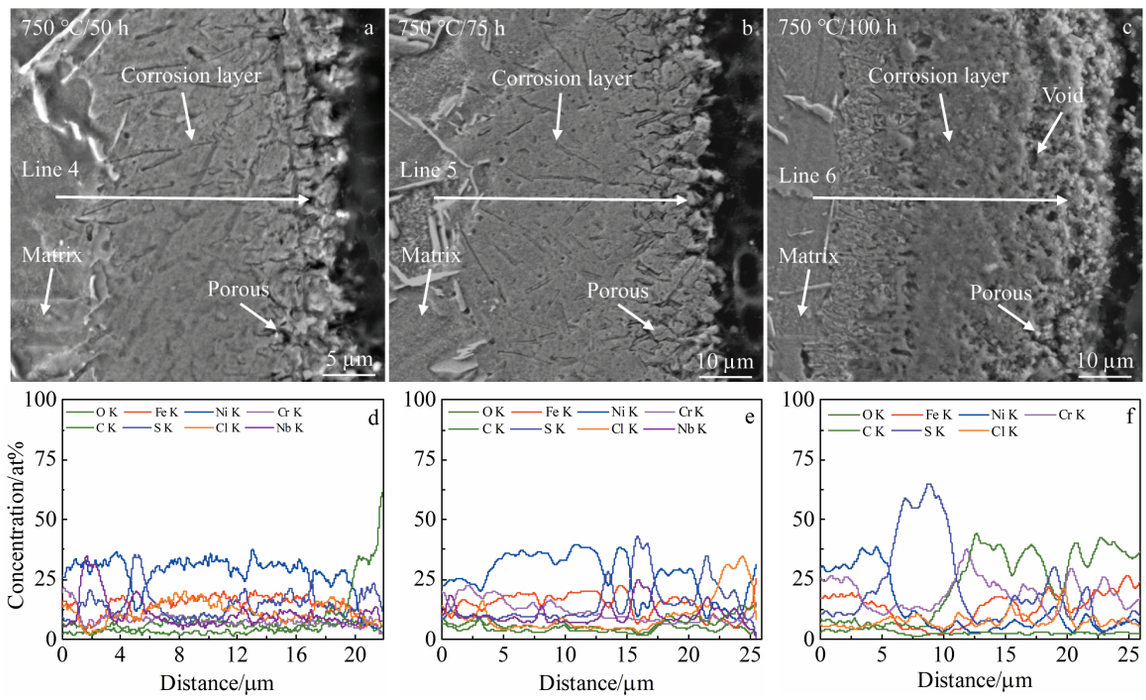

Fig.10 Corrosion oxidation layer morphologies (a~c) and line scan result along line 4 (d), line 5 (e), and line 6 (f) of hot corrosion-treated specimens at 750 °C for different time

of specimens decreases considerably with the increase of temperature, attributing to the transformation of the strengthening phase γ'' into the non-hardening δ phase and the decrease in the γ'' phase (Fig. 6 and 7); as a result, less precipitation hardening is caused. As the heat treatment continues, however, the YS of both corroded and uncorroded specimens shows a slight variation at a certain temperature; this finding is primarily determined by the almost unchanged metallographic appearance. Furthermore, the hot corrosion degrades the YS of the specimens (Fig. 2). At 750 °C , compared with uncorroded specimens, countable needlelike δ phase is generated at grain boundaries of corroded specimens. As generally confirmed in Ref.[26], needle-shaped δ phases in strain-free structure hinder the migration of horizontal grain boundaries to enhance the strength, which can compensate for the decrease in strength because of hot corrosion. Thus, after hot corrosion at a set temperature, the overall YS is elevated slightly except for exposure time of 50 h, at which the enhancement effect cannot reverse the corrosion damage because the content of needle-shaped δ phase is slightly affected by the exposure time of 75 and 100 h, and the values are close. Moreover, as impacted by the defects induced by hot corrosion, more favorable nucleation sites can be created for δ precipitation. As a result, an incremental content of δ phase is identified in the corroded specimens. The variation of UTS is similar to that of YS (Fig.2b), as caused by the same reasons.

At the lowest and the highest testing temperatures (650 and 850 °C), elongation of uncorroded specimens varies slightly as isothermal duration prolongs, which is attributed to less obvious changes of microstructure appearance. However, elongation of corroded specimens declines dramatically at 850 °C, as impacted by an incremental level of degradation with the time. At the treatment temperature of 750 °C, however, the dramatic increase of elongation is presented when the duration increases. It can be suggested that the corroded superalloy exhibits brittle intergranular fracture (Fig. 5b), according with its lowest ductility. The major causes of the occurrence of intergranular fracture are elucidated below. First, for the existence of strengthening phases (γ'' precipitates) in the matrix, the performance of the matrix is relatively great compared with grain boundary. Second, during extension process, the difference of stress between the precipitated δ phases along grain boundaries and matrix without strengthening phase precipitated forms cavities[35]. As a result, the grain boundaries are converted into the preferential sites for crack initiation; then, they undergo the propagation along grain boundaries. Thus, the failure takes place in a mixed ductile and brittle fracture mode under this condition. With the further increase of treatment time, a large number of δ phases precipitate within the matrix, which distinctly reveal the depletion of strengthening phases for their relationship of coexistence, thereby causing the ductile fracture of the specimens, which is accompanied by the increase in elongation.

2.5.2 Corrosion mechanism analysis

The corrosion mechanism from 650 °C to 750 °C follows type-II hot corrosive process, originating from gas induced acid fluxing[9,10]. At 650 °C, sulfate ions enter the matrix through the interstices of the oxide layer and vulcanize nickel

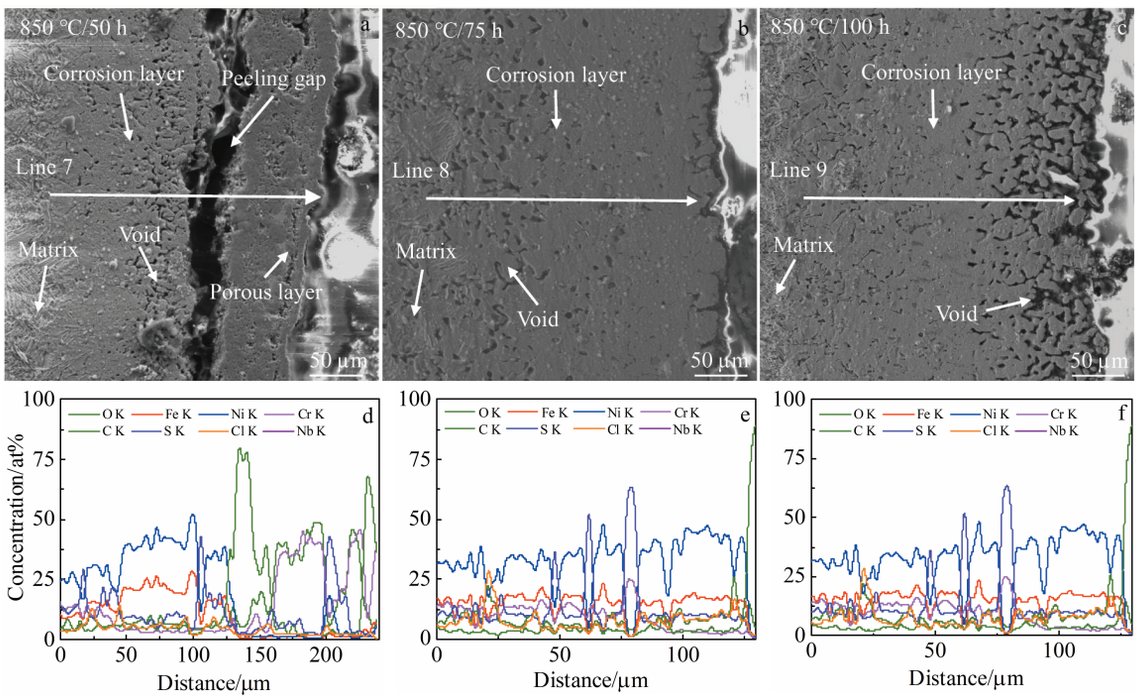

Fig.11 Corrosion oxidation layer morphologies (a~c) and line scan results along line 7 (d), line 8 (e), and line 9 (f) of hot corrosion-treated specimens at 850 °C for different time

in the matrix. At the same time, *M*(Ni, Fe, Cr, etc.) elements in the matrix are oxidized:

$$9Ni + 2SO_4^{2-} \rightarrow 6NiO + 2Ni_3S_2 + 2O^{2-} \quad (1)$$

$$M + x/2O_2 \rightarrow M_2O_x \quad (2)$$

The ongoing oxidizing process of Cr, Fe and other oxidizable elements decrease the oxygen activity, thereby enhancing the activity of S atoms and forming nickel sulfide. Furthermore, nickel sulfide expedites the outward diffusion of Cr and Fe elements and their oxides, thereby leading to the formation of the corrosion layer under the oxide layer. With the hot corrosion proceeding, the corrosion layer gets thicker, the oxygen partial pressure decreases with the oxidation of Cr and Fe, while sulfur partial pressure on surface rises (line 2) and vulcanizes the oxide in corrosion layer. As impacted by the high thermal expansion coefficient of sulfide, significant delamination appears after water cooling. Furthermore, the gas induced by NaCl makes the protective oxide layer porous, increasing the diffusion ratio and concentration of sulfur into the matrix (line 3):

$$2Cr_2O_3 + 5O_2 + 8NaCl \rightarrow 4Na_2CrO_4 + 4Cl_2 \quad (3)$$

With the extension of corrosion time, the surface oxide layer gradually melts, which accelerates the process and makes the corrosion layer much thicker than before. At 750 °C, it conforms to the same corrosion mechanism but with the faster reaction. The protective oxide layer is completely melted (lines 4 and 5) and forms a relatively thick corrosion layer. As the partial pressure of Cl element increases (line 5), *M* elements in the matrix begin to combine with Cl:

$$M + Cl_2 \rightarrow MCl_2 \quad (4)$$

The mentioned metal chlorides are very volatile and will be oxidized again during volatilization and the oxide formed will make the corrosion layer loose (line 6). Until the depletion of overall chloride ions, the oxidation will stop and the chloride ions will eventually volatilize as chlorine gas:

$$2MCl_2 + 3/2O_2 \rightarrow M_2O_3 + 2Cl_2 \quad (5)$$

At 850 °C, the corrosion mechanism varies from type-II to type-I, which is caused by sulphidation, alloy induced acidic fluxing or basic fluxing[9,10]. The sodium sulfate undergoes molten state and decomposes again to form sulfur. The sulfur is easier to enter the matrix than the sulfate ion and directly binds to the *M* elements in the matrix, skipping the mentioned sulfidation and oxidizing process in type-II, which expedites the corrosion:

$$Na_2SO_4 \rightarrow Na_2O + SO_3 \quad (6)$$

$$2SO_3 \rightarrow 2S + 3O_2 \quad (7)$$

$$2M + 3S \rightarrow M_2S_3 \quad (8)$$

After the mentioned process, the thickness of the oxide corrosion layer is elevated significantly. Under the thickness of a certain level, it will peel off after water cooling (line 7). As impacted by the rise of temperature, the rate of chloride oxidation is elevated, and numerous voids appear in the corrosion layer, providing the positions for precipitation of δ phase (lines 8 and 9). Accordingly, the corrosion process refers to a procedure of continuously forming a corrosion layer and subsequently peeling it off.

3 Conclusions

1) The δ content of GH4169 superalloy significantly increases after hot corrosion treatment in comparison with that

of the uncorroded specimen. Moreover, the δ phase of the corrosion specimen is more continuous and coarser in size. This can be due to the porous surface induced by the hot corrosion, which can generate more favorable nucleation sites for δ phase precipitation.

2) The mechanical properties of the GH4169 superalloy exhibit a sensitivity to the precipitation and coarsening of δ phase at grain boundaries, strengthening phases and δ phase within the grains and the transformation of the γ'' phase to the δ phase. Overall, the YS and UTS dramatically decrease, whereas the elongation to fracture increases with increasing the heat treatment temperature. Furthermore, almost all the corroded specimens after the identical treatment present relatively low mechanical properties compared with the uncorroded superalloy, except at 750 ℃.

3) The needle-like brittle δ precipitates at the grain boundaries are proved to effectively boost the tensile strength impacted by the impeded migration of grain boundaries, as well as facilitate the initiation and propagation of intergranular brittle fracture; as a result, ductility is worsened after exposure at 750 ℃.

4) The corrosion mechanism conform to type-II hot corrosion at 650 and 750°C but to type-I hot corrosion at 850 °C. Both of them are the process in which the matrix undergoes the vulcanization, whereas the difference can be reflected by the fact that type-I develops faster than type-II for skipping oxidation. As impacted by the participation of NaCl, the corrosion layer is porous and gradually peels off.

References

1 Tan Y B, Ma Y H, Zhao F *et al. Journal of Alloys and Compounds*[J], 2018, 741: 85

2 Li J, Zhou J Z, Xu S Q *et al*. *Materials Science & Engineering A* [J], 2017, 707: 612

3 Thellaputta G R, Chandra P S, Rao C S *et al. Materials Today Proceedings*[J], 2017, 4(2): 3712

4 Zhao Xinbao, Gu Yuefeng, Lu Jintao *et al. Rare Metal Materials and Engineering*[J], 2015, 44(3): 768 (in Chinese)

5 Hu D, Mao J, Wang X *et al. Engineering Fracture Mechanics*[J], 2018, 196: 71

6 Paramokanetas P, Ozturk U, Calvo J *et al. Journal of Materials Processing Technology*[J], 2018, 255: 204

7 Zhu S, Liu Y, Liu Q *et al. International Journal of Fatigue*[J], 2018: 33

8 He D, Lin Y C, Wang L *et al. Vacuum*[J], 2019, 161: 242

9 Du Jinhui, Lv Xudong, Deng Qun. *Rare Metal Materials and Engineering*[J], 2014, 43(8): 1830

10 Freund L P, Stark A, Pyczak F *et al. Journal of Alloys and Compounds*[J], 2018, 735: 333

11 Cao G H, Sun T Y, Wang C H *et al. Materials Characterization* [J], 2018, 136: 398

12 Lin Y C, Wu X, Chen X *et al. Journal of Alloys and Compounds* [J], 2015, 640: 101

13 He D, Lin Y C, Jiang X *et al. Materials & Design*[J], 2018, 156: 262

14 Lass E A, Stoudt M R, Williams M E *et al. Metallurgical and Materials Transactions A*[J], 2017, 48(11): 5547

15 Anderson M, Thielin A L, Bridier F *et al. Materials Science and Engineering A*[J], 2017, 679: 48

16 He D, Lin Y C, Tang Y *et al. Materials Science and Engineering A*[J], 2019, 746: 372

17 Pradhan D, Mahobia G S, Chattopadhyay K *et al. Materials Today: Proceedings*[J], 2018, 5(2): 7047

18 Geng Y, Dong X, Wang K *et al. Surface & Coatings Technology* [J], 2019, 370: 244

19 Li S, Yang X, Qi H *et al. International Journal of Fatigue*[J], 2018, 116: 334

20 Bradshaw A, Imms N J, Nicholls J R *et al. Surface & Coatings Technology*[J], 2013, 228: 248

21 Pradhan D, Mahobia G S, Chattopadhyay K *et al. International Journal of Fatigue*[J], 2018, 114: 120

22 Mahobia G S, Paulose N, Mannan S L *et al. Journal of Materials Engineering and Performance*[J], 2013, 22(12): 3810

23 Zhang S, Zhang H, Cheng M *et al. Materials Science and Engineering A*[J], 2011, 528(19): 6253

24 Lin Y C, Deng J, Jiang Y *et al. Materials Science and Engineering A*[J], 2014, 598: 251

25 Ye N, Cheng M, Zhang S *et al. Journal of Iron and Steel Research International*[J], 2015, 22(8): 752

26 Zhang H, Li C, Guo Q *et al. Materials Science and Engineering A*[J], 2018: 136

27 Homaeian A, Alizadeh M. *Engineering Failure Analysis*[J], 2016, 66: 373

28 Wang P, Yu Z, Zhang Y *et al. Material Science & Technology*[J], 2018, 26(6): 36 (in Chinese)

29 Elawadi G A, Abdelsamad S, Elshazly E S *et al. Applied Surface Science*[J], 2016, 378: 224

30 An X L, Zhang B, Chu C L *et al. Materials Science and Engineering A*[J], 2019, 744: 255

31 Babu K A, Mandal S, Kumar A *et al. Materials Science & Engineering A*[J], 2016, 664: 177

32 Chen F, Cui Z S, Ou H G *et al*. *Applied Physics A*[J], 2016, 122: 890

33 Zhang H, Li C, Guo Q *et al. Materials Characterization*[J], 2017, 133: 138

34 Lin Y C, He D, Chen M *et al. Materials & Design*[J], 2016, 97: 13

35 Shen Jialin, Wei Xianyi, Xu Pingwei *et al. Rare Metal Materials and Engineering*[J], 2019, 48(5): 1467 (in Chinese)

热腐蚀对GH4169高温合金δ相析出和拉伸性能的影响

宋肖肖[1]，周　律[1]，李　柯[1]，任凯旭[2]，王加余[2]，王　鑫[2]

(1. 中国民航大学 中欧航空工程师学院，天津 300300)

(2. 中国汽车技术研究中心有限公司，天津 300300)

摘　要：分别在650、750、850 ℃热处理条件下，研究了高温合金GH4169在75Na_2SO_4+25NaCl（质量分数）熔盐环境下的热腐蚀行为，之后进行组织表征和力学性能测试。结果表明：随着热处理温度的不断升高，高温合金的抗拉极限强度（UTS）和屈服强度（YS）都出现急剧退化，伸长率显著提高。但在750 ℃条件下，晶界处析出的针状δ相能提高高温合金的强度，导致合金出现沿晶脆性断裂现象，降低了合金的塑性。在650和750 ℃下，腐蚀机理符合II型热腐蚀，但在850 ℃条件下符合I型热腐蚀，2种不同类型腐蚀都促进了基体δ相的析出。

关键词：热腐蚀；GH4169高温合金；δ相；拉伸性能

作者简介：宋肖肖，男，1990年生，硕士，中国民航大学中欧航空工程师学院，天津 300300，电话：022-24092872，E-mail：xxsong@cauc.edu.cn